Journal of Materials Chemistry A

Accepted Manuscript

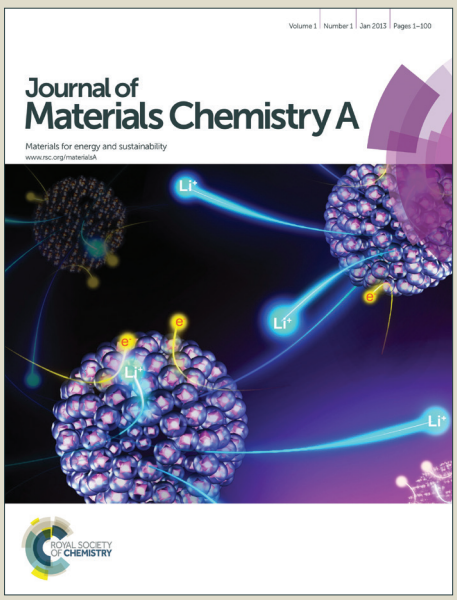

ROYAL SOCIETY OF CHEMISTRY

www.rsc.org/materialsA

Journal Name

RSCPublishing

ARTICLE

Electrochemical reduction of $Ag_2VP_2O_8$ composite electrodes visualized via *in situ* Energy Dispersive X-Ray Diffraction (EDXRD): unexpected conductive additive effects

Cite this: DOI: 10.1039/x0xx00000x

Received ooth January 2012,
Accepted ooth January 2012

DOI: 10.1039/x0xx00000x

www.rsc.org/

Kevin C. Kirshenbaum[a, b, c], David C. Bock[b], Zhong Zhong[a], Amy C. Marschilok[b,c]*, Kenneth J. Takeuchi[b,c]*, Esther S. Takeuchi[a,b,c]*

In this study, we characterize the deposition of silver metal nanoparticles formed during discharge of Li/$Ag_2VP_2O_8$ cells with composite cathodes containing conductive carbon additive. Using *in situ* energy dispersive x-ray diffraction (EDXRD) of an intact battery, the location and distribution of silver metal nanoparticles generated upon reduction-displacement deposition within an $Ag_2VP_2O_8$ cathode containing a pre-existing percolation network can be observed for the first time. This study yielded unexpected results where higher rate initial discharge generated a more effective conductive matrix. This stands in contrast to cells with cathodes with no conductive additive where a low rate initial discharge proved more effective. These results provide evidence that using conductive additives in conjunction with an *in situ* reduction-displacement deposition of silver metal provides a path toward the ultimate goal of complete electrical contact and full utilization of all electroactive particles.

Broader Context

Batteries designed for high power, high energy density applications require electrodes with high electrical conductivity in order to enable full utilization of the electroactive material. The most effective electrode structure would provide electronic contact of each electrochemically active particle. The most common approach for forming a conductive network is to incorporate a conductive additive such as carbon in the composite electrode. An alternative successful strategy for the enhancement of electrical conductivity of an electrode is through the use of an electroactive polyanion framework containing silver cations ($Ag_2VP_2O_8$) which can be discharged via a reduction-displacement mechanism, forming *in situ* conductive silver metal deposits upon initial discharge. The silver metal particles formed on the surfaces of the active material particles can effectively link to generate a percolation network within the cathode. In the results presented here, both strategies are used in concert demonstrating an unexpected rate dependence for the formation of the conductive network. Further, we present methodology demonstrating that through use of a combination of experimental techniques, it is possible to determine the conditions under which an optimal electrically conductive network can be formed, a strategy which can be extended to other materials.

Introduction

Improving access of the total electrical capacity in an electrode remains an important area of battery research.[1] Presently, commercial battery systems utilize composite electrodes containing conductive additives to improve electrical contact between the electroactive material and the current collector with the intent of 'wiring' each particle of active material. The current method for preparing electrodes depends on uniform dispersion of the appropriate ratio of electroactive and conductive materials and the formation of an electrically conductive percolation network of conductive additive particles. However, the standard electrode fabrication approach may not be fully successful in achieving homogeneous and complete contact with each electroactive particle.[2, 3] This can then lead to hindered electron access to regions of the electrode and prevent full utilization of capacity, particularly under high current conditions.

Our paradigm for creating sufficient electrical contacts between all active material particles is to electrochemically generate *in situ* a conductive network of metal nanoparticles in the electrode through a reduction-displacement reaction. For example, electrolytes with $AgPF_6$ additives have been shown to deposit silver metal on the surface of graphite anodes and improve performance at higher discharge rates.[4] Similarly, to reduce the necessity of additives, we previously demonstrated that upon discharging silver vanadium phosphorous oxide (SVPO, $Ag_wV_xP_yO_z$) cathodes, silver metal nanoparticles form and populate the surfaces of the SVPO particles, forming a 3-dimensional conductive matrix.[5, 6] Notably, SVPO materials are highly resistive and can be considered as an insulators prior to discharge. For example, upon reduction-displacement, the silver metal nanoparticles deposit on the surfaces of an $Ag_2VO_2PO_4$ material, resulting in a decrease in the measured impedance of the $Li/Ag_2VO_2PO_4$ electrochemical cell by 15000 upon initial discharge.[5] Conceptually, the particles of SVPO are insulators surrounded by silver metal nanoparticles, which are conductors. This study focuses specifically on $Ag_2VP_2O_8$, another member of the SVPO material family. Based on typical sizes of the $Ag_2VP_2O_8$ particles and silver metal particles, we estimate that at 0.1 electron equivalents of reduction, the volume of silver metal is ~1.1% of the total volume,[7] exceeding the minimum percolation threshold of 0.3% for a carbon-free $Ag_2V_2O_8$ cathode.[8] Notably, a percolation network is necessary but not sufficient to ensure full utilization of an electroactive material. Thus, to fully access every electroactive particle, the reduction-deposition mechanism must be further investigated and understood, with the ultimate goal of establishing complete electrical contact with every particle.

Towards that end, we have previously explored the reduction-deposition of silver metal in electrodes of pure, carbon-free $Ag_2VP_2O_8$[6, 7] using *in situ* energy dispersive x-ray diffraction (EDXRD) measurements to create a tomographic profile showing the spatial distribution of silver in the electrodes. This technique has been used recently to study structural changes in the cathode material as a function of depth of discharge for a range of battery systems.[9-13] Additionally, the rate by which the material discharges has a significant effect on spatial distribution of deposited silver particles; in a recent study we observed that slower discharge rates resulted in more uniform silver metal distribution throughout electrodes of pure $Ag_2VP_2O_8$.[14]

Our previous studies were performed on electrodes of pure, carbon-free active material, where the *in situ* formation of silver metal was initiated within an electronically insulating parent electrode, which then showed dramatic changes in the conductivity of the electrode as a function of discharge. In the current report, sufficient conductive additive (carbon) was dispersed among the active material to form a conductive network of carbon within the electrode prior to electrochemical reduction. This enabled the first *in situ* visualization of the reduction-deposition of silver metal upon partial reduction of $Ag_2VP_2O_8$ progressed in the presence of a pre-existing conductive carbon percolation network.

Specifically, the effect of carbon additives in a composite electrode is to provide conductive pathways for electron access, however this study directly demonstrates that that simply reaching a percolation threshold in an electrode is not sufficient. In addition to decreasing the overall resistance of the electrode, the conductive networks in an electrode containing a nonconducting active material must provide conducting pathways to each electroactive particle to allow for full utilization of the active material. The challenge with regard to electrode design is how to do this volumetrically efficiently.

In a previous study, different amounts of carbon (from 2-10 wt%) were added to $LiCoO_2$ and $LiMn_2O_4$ cathodes.[15] The authors found that although the lower carbon content is sufficient to increase the conductivity of the electrode, the utilization of the active material increased with the further addition of conductive additives, pointing to the importance of carbon-to-active material contact. In a similar study, Hong et al. found that different types of carbon mixed with $LiCoO_2$ create composite electrodes with different electrochemical performance.[16] Increasing the carbon/LiCoO2 interface area reduced polarization and provided a more complete utilization of the cathode. These studies showed that it is not simply the bulk electrode conductivity that affects the utilization but also the local interparticle conductivity that is important.

In this study, we perform EDXRD measurements on coin cells with $Ag_2VP_2O_8$ electrodes including conductive carbon as part of the electrode formulation. The $Li/C\text{-}Ag_2VP_2O_8$ cells were first characterized using the *in situ* techniques of AC impedance and EDXRD. The electrodes were subsequently removed from the cells for *ex situ* measurements by x-ray powder diffraction and x-ray absorption spectroscopy to further characterize the silver metal formation. The results presented here demonstrate that 1) a pre-formed percolation network of conductive carbon does not create an ideal conductive network which would enable full utilization of the electroactive material; and 2) the presence of a pre-formed percolation network does improve the homogeneity of the reduction-

displacement deposition process, promoting formation of a more even distribution of silver metal deposits upon electrochemical reduction-displacement. The results presented provide evidence that using conductive additives in combination with an *in situ* reduction-displacement deposition of silver metal provides a new strategy towards the ultimate goal of complete electrical contact and full utilization of all electroactive particles with an electrode. This study yielded unexpected results where higher rate initial discharge generated a more effective conductive matrix. This stands in contrast to cells with cathodes with no conductive additive where a low rate initial discharge proved more effective.[14] Further, we present methodology demonstrating that through use of a combination of experimental techniques, it is possible to determine the conditions under which an optimal electrically conductive network can be formed.

Experimental

$Ag_2VP_2O_8$ was synthesized using a solid state reaction previously reported in the literature.[17] X-ray diffraction measurements were performed using a Rigaku Smart Lab XRD system with Cu Kα radiation. The synthesized material matched the reference pattern (PDF 01-088-0436) with no impurity phases detected. Active material was mixed with 15% (by weight) of graphite (Timcal) before being formed into cathodes. This amount of graphite is considerably higher than the observed percolation threshold for materials with similar particle sizes, thus the effects of creating a conductive network should be minimized, allowing measurements to focus on changes to the conductivity at a particle level.[18, 19] Stainless steel coin cells were fabricated using the cathodes, Li metal anodes, polymer membrane separators, and an electrolyte consisting of ethylene carbonate and dimethyl carbonate with 1 M $LiPF_6$.

Coin cells were discharged to 0.1, 0.5, or 1.0 electron equivalents at a rate of either C/168 (full discharge in 168 hours, what will be referred to as the faster discharge rate) or C/1440 (slower discharge rate). Before and after discharge, electrochemical impedance spectroscopy measurements were obtained from 0.5 mHz to 100 kHz at 30 °C using a VSP potentiostat from Bio-Logic.

In situ energy dispersive x-ray diffraction (EDXRD) measurements were performed on intact discharged cells at beamline X17B1 of the National Synchrotron Light Source (NSLS-I) at Brookhaven National Laboratory. A white x-ray beam (approx.. 50 – 200 keV) was narrowed to a height of 20 μm, and the coin cells were placed on a moveable stage so that diffraction patterns as a function of position within the cell could be measured. The detector was placed at $2\theta = 3.05°$ and the receiver slits were set so that the gauge volume for each spectrum was 2 x 2 x 0.02 mm^3. A description of the experimental setup and EDXRD technique including figures has been published elsewhere.[2, 7]

Following the EDXRD measurements, the coin cells were disassembled and the cathodes were rinsed with dimethyl carbonate, dried, and ground to measure spatially averaged properties. Angle-resolved x-ray diffraction (XRD) patterns were measured and peaks in the diffraction patterns were fit using Jade software.

Samples for x-ray absorption measurements were prepared by mixing the cathode material with graphite and pressing the mixture into a pellet such that the thickness of the pellet was equal to one absorption length at the measured energy. X-ray absorption spectroscopy (XAS) at the Ag K-edge was measured at beamline X11A at NSLS-I using Ag foil as a reference standard. The resulting spectra were normalized and aligned using the reference foil with the ATHENA software package.[20] Linear combination fitting (LCF) was performed using ATHENA software using Ag metal and $Ag_2VP_2O_8$ powder as the end members.

Scanning electron microscopy images were obtained to further characterize the size of the Ag^0 particles which formed during discharge. The graphite containing cathode pellets were recovered from the cells and ground prior to SEM. Backscattered electron (BSE) mode was used to achieve good contrast between the higher atomic number Ag^0 particles and the discharged $Ag_2VP_2O_8$ particles. For over 300 individual Ag^0 particles were measured using imageJ software. The public domain Java image processing program Image J[21] was used to analyze the size of the Ag^0 particles. Volume weighted distributions of the Ag^0 particles in each sample were determined assuming spherical shape for the Ag^0 particles.

Results

AC Impedance Spectroscopy

The results of AC impedance spectroscopy measurements of the coin cells are presented in Fig. 1. Figs. 1(a) and (b) show the absolute value of the impedance as a function of frequency before and after discharging, respectively. Before discharging, there are small differences in the impedance of the cells at higher frequencies, however these differences amount to less than a few ohms. Similarly, at low frequencies there are only very small variations in the impedance: at 1 mHz the impedance is 3278 ± 53 Ω across all cells. After discharge, the frequency response of the cells remain similar to one another, with the most significant differences arising in the absolute value of the impedance at frequencies below 0.1 Hz. Fig. 1(c) shows that all cells exhibit the same features in the AC response with a large portion of the differences occurring only a slight shift in the Z' intercept at high frequency and the absolute value of the impedance at low frequency.

At the lowest frequencies, |Z| is dependent on the depth of discharge [see Fig. 1(b)], consistent with the formation of Ag nanoparticles [5]. In the cell discharged to 1.0 electron equivalents, the low-frequency impedance decreases by a factor of about 20, a much smaller effect than is seen in cells without conductive additives. Pure $Ag_2VP_2O_8$ is insulating and thus the formation of silver metal nanoparticles greatly enhances the conductance; in previous studies on cathodes without

conductive additives, discharging to 0.5 electron equivalents decreased the impedance by a factor of ca. 500 [2, 7]. Here we see that with the addition of graphite to the cathode pellet the impedance of the cell is greatly reduced, notably the effect of additional conductive material

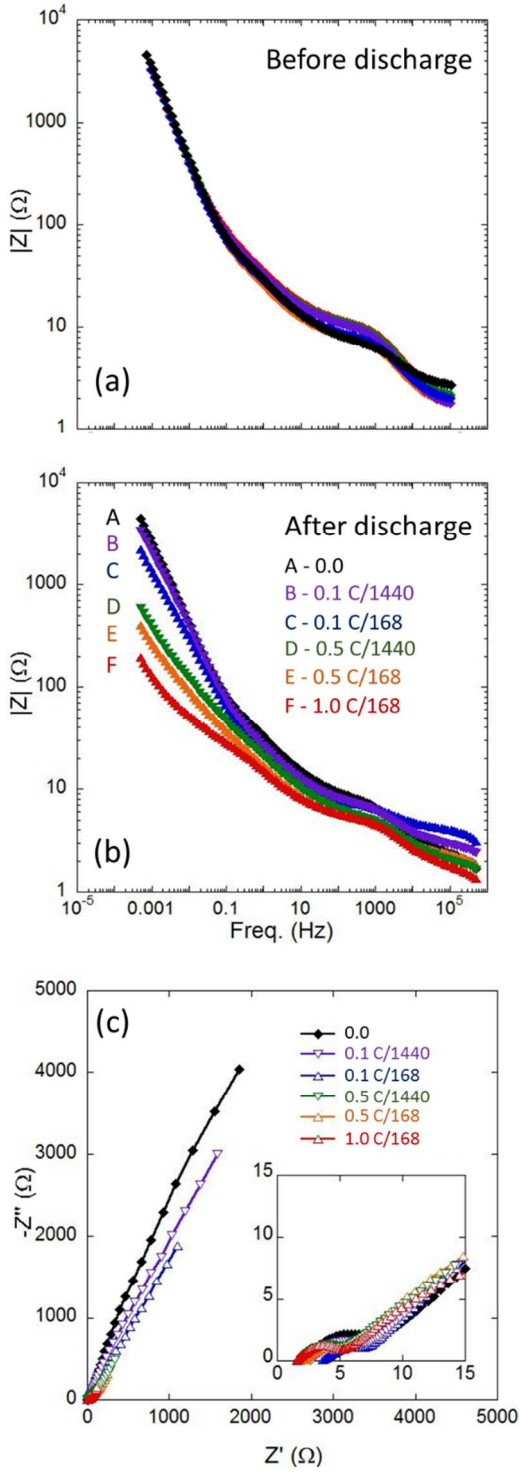

Figure 1: AC impedance results for coin cells with $Ag_2VP_2O_8$ cathodes with 15 wt% graphite, before and after discharging. (a) Absolute value of the AC impedance as a function of frequency for coin cells before discharge. The low frequency impedance of the cells differs by less than a few percent. (b) Absolute value of the AC impedance as a function of frequency for coin cells after discharge. The individual datasets are labeled with the depth of discharge and C-rate, meaning that the cells were discharged at the faster (C/168) or slower (C/1440) rates, respectively. The impedance is lower for cells discharged to greater depths, and for cells discharged at faster rates. (c) Nyquist plot of the AC impedance response of the cells after discharge. The inset shows the high frequency region.

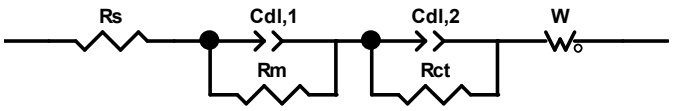

Figure 2: Equivalent circuit model used for fit.

DOD, Rate	0	0.1, C/1440	0.5, C/1440	0.1, C/168	0.5, C/168	1.0, C/168
R_s	2.15(1)	2.77(1)	1.90(1)	3.87(2)	2.24(2)	1.64(1)
R_m	4.21(5)	3.16(4)	2.51(5)	2.04(5)	2.05(8)	3.02(10)
R_{ct}	1705(155)	1213(46)	170(39)	566(24)	219(181)	34(2)

Table 1: Results of fit of AC impedance data to resistance elements of equivalent circuit model.

(silver metal formation) on the overall conductivity is still apparent, showing a factor of 10 difference between the impedance of the non-discharged cells and the cells discharged to 0.5 electron equivalents.

The changes in impedance are telling about the effect of discharge rate on silver formation. We determined that in $Li/Ag_2VP_2O_8$ cells without graphite less Ag^+ was reduced at the faster discharge rate in favor of V^{n+} reduction.[2] This led to the observation of a low frequency impedance that was approximately 4 times greater in the cell discharged at the faster rate. The cells in this work include graphite as a conductive additive and we will show that, unlike the previous studies, the amount of silver metal formed is comparable at both discharge rates. Therefore, the differences in the AC impedance response for $Li/C\text{-}Ag_2VP_2O_8$ cells discharged at different rates is not due to the amount of silver ion that is reduced, but rather to the size of the silver metal particles formed and the effectiveness of the conductive network in promoting interparticle contact.

The AC impedance data were fit to an equivalent circuit model, Fig. 2. Selected results from the fit are shown in Table 1, complete results are shown in Table S1. In this model, Rct refers to the charge-transfer resistance of the cathode, a measure of the interparticle resistance. We find that the charge transfer resistance decreases as a function of DOD as expected from the increase in metallic silver. We also find that at a depth of discharge of 0.1 electron equivalents the charge transfer resistance is approximately half in the cell discharged at the faster rate (C/168) as compared to that discharged at the slower rate (C/1440). This charge transfer resistance is closely tied to the rate capability: in a study on another insulating phosphate material, $LiFePO_4$, coating the $LiFePO_4$ particles with different types of carbon was shown to dramatically improve the capacity and rate capability in composite electrodes.[22] Interestingly, different types of carbon coating were shown to

give different charge transfer resistances, and the electrodes with the lowest charge transfer resistances showed a higher capacity at increased discharge rates in the $LiFePO_4$ study. Our results suggest that by discharging at a faster rate earlier in the lifetime of the cell it may be possible to decrease the charge transfer resistance of $Ag_2VP_2O_8$ and thereby improve the rate capability and thus the pulse current capability.

Energy Dispersive X-Ray Diffraction

EDXRD has been demonstrated as an effective tool for the in situ interrogation of mechanisms within energy storage systems.[9, 23, 24] Using an in situ EDXRD technique, we measured diffraction spectra for coin cells every 20 μm through the thickness of the cathode. Fig. 3 presents a 3D overlay of half of the measured spectra (i.e., 40 μm increments) through the cathode, with blue hues representing data taken closer to the Li anode (lower beam position), and red hues for data taken closer to the stainless steel coin cell top (higher beam postion). The red dashed line in the 3D overlays shows the position of the Ag(111) peak at 1/d=0.4239 $Å^{-1}$. The average intensity of three $Ag_2VP_2O_8$ peaks (at 1/d = 0.5130, 0.5303, 0.5506 $Å^{-1}$) and the intensity of the Ag(111) peak are plotted as a function of beam position next to the 3D overlays, with black, closed symbols for the $Ag_2VP_2O_8$ intensity and red, open symbols for Ag. The discharge conditions of the cathodes in this figure are as follows: (a) pure $Ag_2VP_2O_8$ discharged to 0.1 elec. equiv., (b) $Ag_2VP_2O_8$ with 15 wt% graphite discharged to 0.1 elec. equiv., (c) pure $Ag_2VP_2O_8$ discharged to 0.5 elec. equiv., and (d) $Ag_2VP_2O_8$ with 15 wt% graphite discharged to 0.5 elec. equiv. All of the cells in this figure were discharged at a rate of C/1440.

Cells without graphite (Figs. 3(a) and (c)) show a distribution of silver that is asymmetric within the cathode with the highest silver concentration occurring on the side closest to the steel coin cell (further from the Li).[7] These results highlight the importance of the silver conducting network that is formed on discharge: in cells without graphite, the limiting factor in the discharge is access to electrons, causing uneven discharging and potentially limiting the realizable discharge capacity.

With the addition of graphite (Figs. 3(b) and (d)), we see that the intensity of the Ag(111) peak changes proportionally to $Ag_2VP_2O_8$ peak intensity through the thickness of the cathode, pointing to a much more spatially even discharge profile. By including a conductive additive, in this case graphite, we can see that the discharge is no longer limited by electron access as in the case of cathodes without graphite. Additionally, the fact that the amount of silver metal is even throughout the cathode indicates that at these rates Li ion diffusion is fast enough to allow for even discharge.

In Fig. 4 we show peak intensity as a function of beam position for cathodes with graphite discharged at C/168 (faster rate) and C/1440 (slower rate) to multiple depths. The figure shows the intensities of the stainless steel (211) peak in light grey, the Ag(111) peak in red, and the average of three $Ag_2VP_2O_8$ peaks in black. The Li diffraction peaks are not pictured as they are only intermittently visible due to recrystallization of the Li foil during processing [25, 26]. The background of each plot is shaded to show the approximate positions of the various parts of the battery; from top to bottom the parts are: steel coin cell casing, cathode pellet, polymer separator, and Li anode. The peak in the intensity of silver metal around beam position of 2.1 mm in each cell is attributed to the presence of silver metal on the surface of the Li anode, most

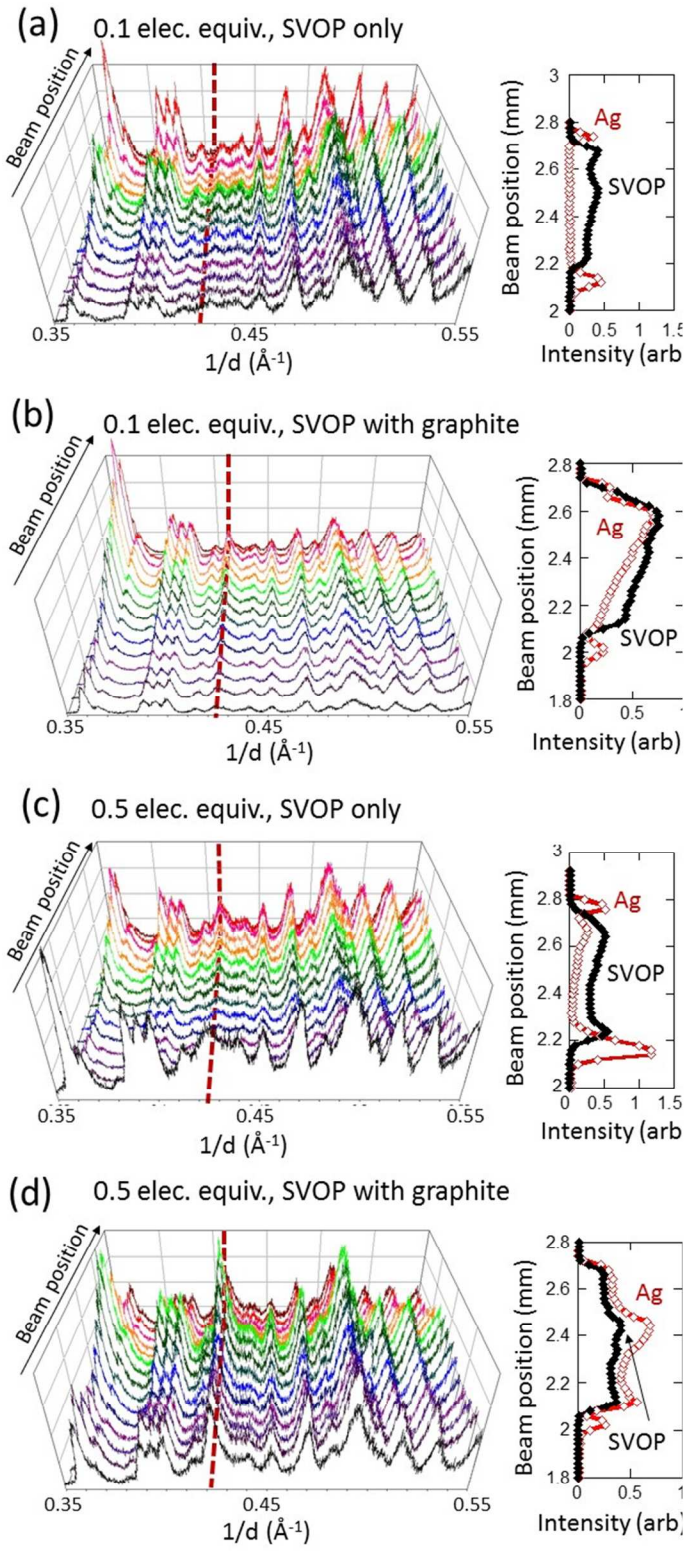

Figure 3: 3D overlays of EDXRD spectra obtained within the cathode along with the Ag and $Ag_2VP_2O_8$ peak intensities as a function of beam position through the coin cell for different cell conditions: (a) pure $Ag_2VP_2O_8$ cathode discharged to 0.1 elec. equiv., (b) $Ag_2VP_2O_8$ with 15 wt% graphite discharged to 0.1 elec. equiv., (c) pure $Ag_2VP_2O_8$ discharged to 0.5 elec. equiv., (d) $Ag_2VP_2O_8$ with 15 wt% graphite discharged to 0.5 elec. equiv.

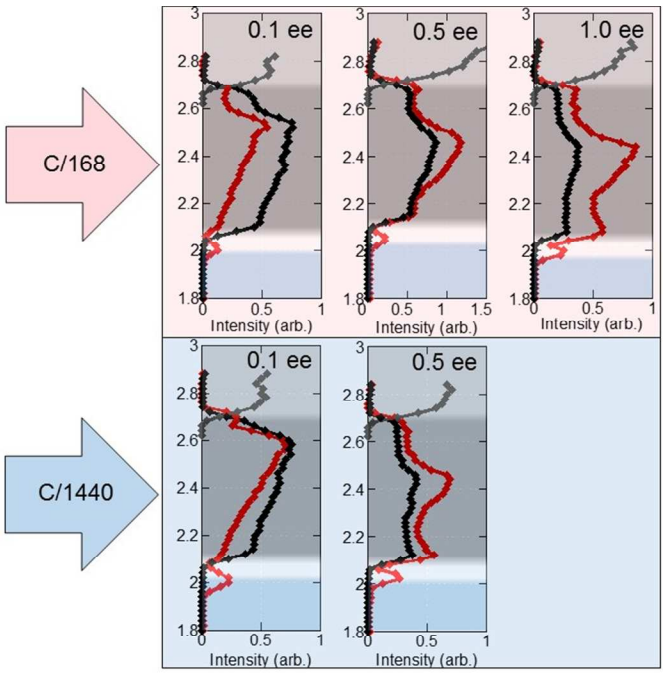

Figure 4: Intensity of peaks measured by EDXRD as a function of beam position for cells with $Ag_2VP_2O_8$/Graphite cathodes. Cells were discharged to 0.1, 0.5, and 1.0 elec. equiv. at C/168 (fast discharge rate) or C/1440 (slow discharge rate). The intensities included in the figure are: stainless steel (211) peak (light grey), the Ag(111) peak (red), and the average of three $Ag_2VP_2O_8$ peaks at 1/d = 0.5130, 0.5303, 0.5506 $Å^{-1}$ (black). The shaded background shows the approximate positions of the steel, cathode pellet, polymer separator, and Li anode.

likely due to Ag^+ dissolution in the electrolyte and subsequent reduction on the Li interface [2, 27, 28].

The overall intensity of the Ag(111) relative to the $Ag_2VP_2O_8$ peaks increases as a function of DOD as expected. In addition to peak intensity, we use XRD peak area as well as XAS measurements to further quantify the relative amounts of silver. Ultimately, we will show that the difference between peak intensity and area comes from differences in the silver particle size, and that these differences are driving the changes in the AC impedance response.

Ex situ X-Ray Diffraction

To further clarify the amount and size of Ag crystallites, we removed the cathodes from the cells and measured x-ray diffraction patterns after regrinding the pellets. Fitting the Ag(111) peak shows that the shape does not match a typical Voigt or Pearson-VII lineshape, likely due to a distribution of silver metal crystallite sizes. Because the crystallite sizes (and therefore peak widths) are variable, the area of the Ag(111) peak should be more accurate than the peak intensity in obtaining the amount of silver metal in the cathode. In our previous work we showed that the Ag(111) peak area and the x-ray absorption spectrum of the Ag edge give similar results and can be used to determine the amount of silver metal present in the discharged cathode [2]. In Fig. 5(a) we see that the total area under the peak is equivalent for fast and slow discharge rates in cathodes with graphite and falls between that observed for cells without graphite discharged at the two rates.

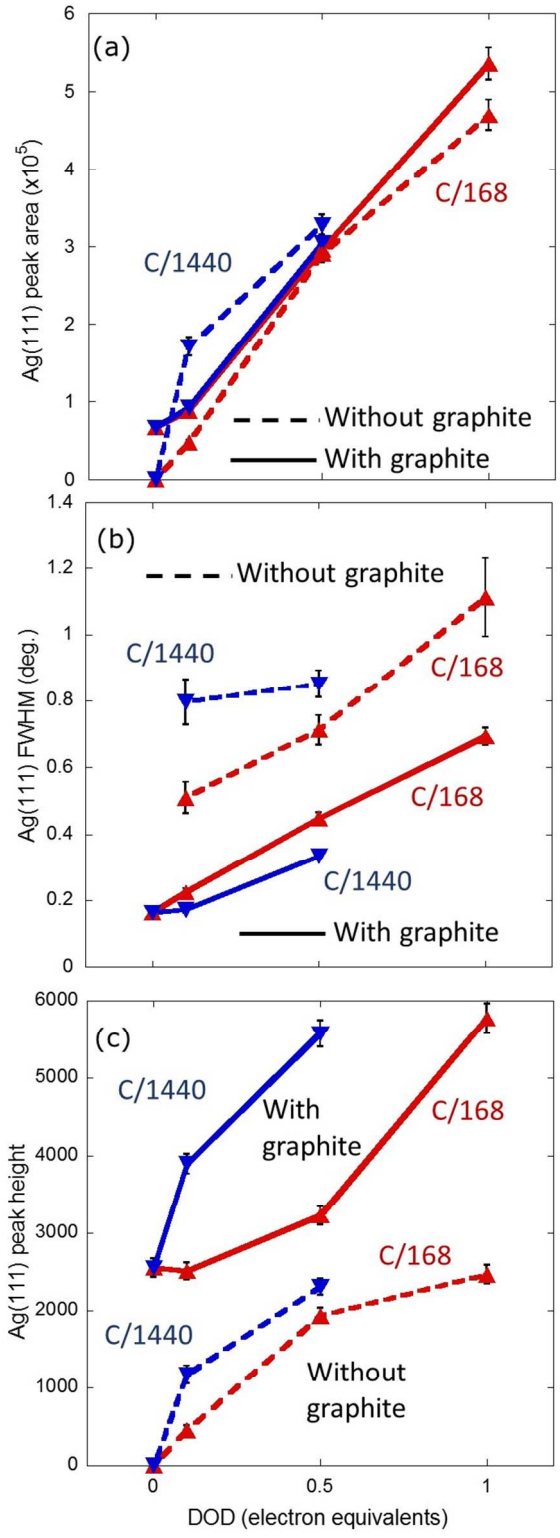

Figure 5: Analysis of ex situ XRD measurements of discharged cathode pellets with (solid lines) and without graphite (dashed lines). Data for cells discharged at the faster rate, C/168, are in red and marked with triangles while cells discharged at the slower rate, C/1440, are in blue and marked with upside-down triangles. (a) Area of the Ag(111) peak. (b) FWHM of Ag(111) peak. (c) Peak intensity of the Ag(111) peak. The amount of silver metal in the cells with graphite is independent of discharge rate, however the crystallite size is smaller in the cells discharged at the faster rate.

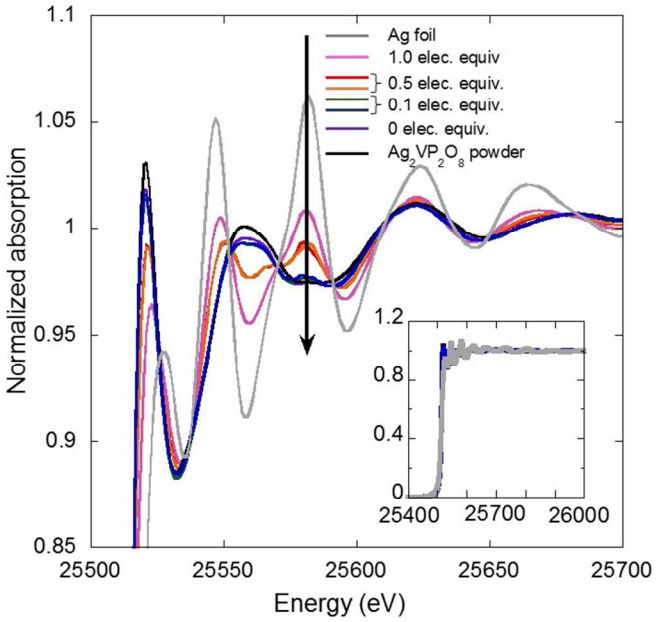

Figure 6: Normalized x-ray absorption spectrum of the Ag K-edge in the near-edge region. Spectra were obtained for the discharge rates/depths discussed in previous sections. Inset: full range of spectra showing the K-edge.

Although the amount of silver metal is consistent between the two discharge rates, the FWHM of the peak and height (intensity) of the peak (Figs. 5(b) and (c), respectively) are very different, indicating that the average crystallite size depends greatly on the discharge rate. The peak width is much smaller for the cells with graphite than those without. This discrepancy between the size of Ag nanoparticles may be due to the improved electron access due to the conductive additive. In electrodes with poor electronic conductance, the local electron access will be more random. By increasing the electron access, it is possible to have regions discharge that receive a steady flow of electrons that can be used to reduce the cathode.

In the cells with graphite, the FWHM is greater in cells discharged at the faster rate and thus the Ag particles are smaller. The FWHM values reported in Fig. 5(b) correspond to Ag crystallite sizes of approx. 40 nm for the cells discharged to 0.1 elec. equiv. to 11 nm in the cell discharged to 1.0 elec. equiv. Despite having the same amount of silver metal through the cathode, as we saw in a previous section, the AC impedance at low frequencies showed that the cells discharged at the faster rate were more conductive than those discharged at the slower rate. From the ex situ XRD results, we can see that the silver crystallite size also plays a role in creating an effective conducting network, rather than only the volume of silver metal. The smaller crystallites observed at the faster discharge rate would more effectively cover the insulating $Ag_2VP_2O_8$ particles and produce a better network of conducting Ag nanoparticles, reducing the impedance of the cathode.

Scanning electron microscopy (SEM) images were obtained to characterize the size of the Ag^0 particles which formed during discharge of the graphite containing cathode pellets.

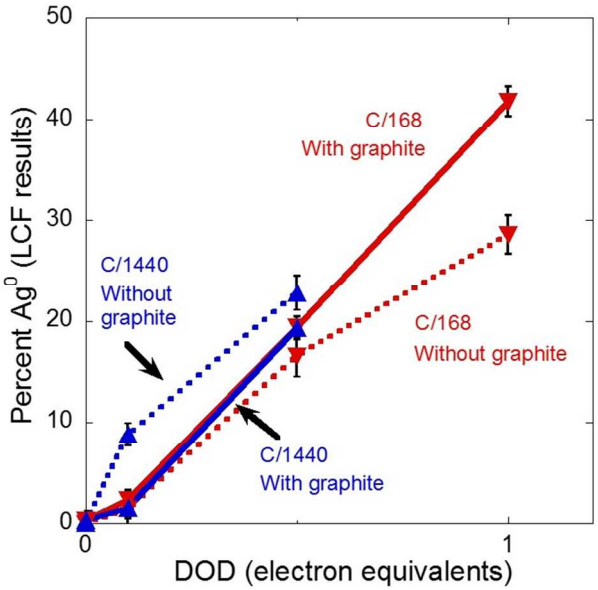

Figure 7: Linear combination fitting (LCF) results of Ag K-edge x-ray absorption data for cells with (solid lines) and without graphite (dashed lines). The amount of silver metal in each cathode as determined by LCF matches the Ag(111) peak area obtained by XRD. The amount of silver metal is independent of discharge rate for the cells with graphite.

Representative SEM images (Fig. S1) and volume weighted distributions of the Ag^0 particles in each sample (Fig. S2) are provided as Supplemental Information. For all samples investigated by SEM, > 75% of the Ag^0 particle volume was contained in particles greater than 50 microns in size. Since Ag^0 crystallite size calculated by XRD Scherrer analysis ranged from 11 to 40 nm depending on the sample, these results indicate that multiple crystallites compose a particle of Ag^0 in each case.

X-Ray Absorption Spectroscopy

Fig. 6 shows the x-ray absorption spectra at the Ag K-edge for the discharged $Ag_2VP_2O_8$/graphite material along with as synthesized $Ag_2VP_2O_8$ powder and a silver metal foil as reference materials. The absorption spectra for the cells discharged to the same elec. equiv. (0.1 or 0.5) at the two discharge rates (C/168 or C/1440) are nearly indistinguishable.

When plotted together, the post-edge regions show numerous isosbestic points (points of equal absorption among all of the samples), indicating a transition of the Ag atoms between exactly two states: Ag^+ and silver metal.[29] Because of this, linear combination fitting (LCF) can be used to determine the ratio of
silver metal to Ag^+ in the discharged cathodes [30]. Fig. 7 presents the results of linear combination fitting in the cells with graphite (solid lines) and compares them to the previously reported results for cells without graphite (dashed lines). We find that the silver metal content increases with DOD and is independent of discharge rate. These results are in agreement with the Ag(111) peak area measured by XRD presented in the previous section. The percentage of silver metal in the cells with graphite falls between that of the cells without graphite discharged at the two different rates.

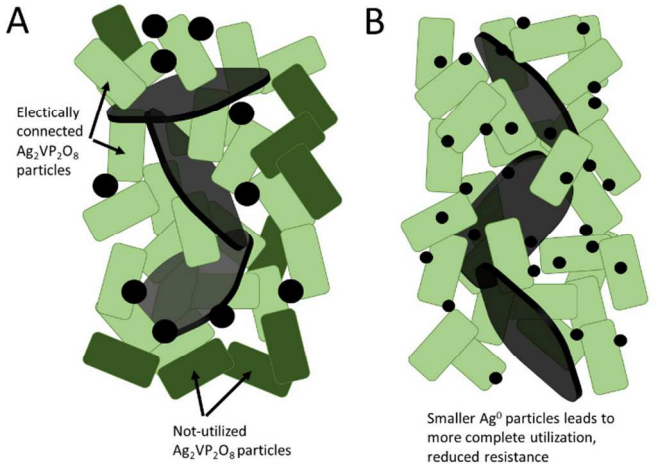

Figure 8: Conceptual figure depicting $Ag_2VP_2O_8$ cathode discharged under (A) slower and (B) faster discharge rates, where light green represents electrically connected $Ag_2VP_2O_8$ particles, dark green represents non-utilized $Ag_2VP_2O_8$ particles, and black represents Ag^0 particles formed *in situ* as a result of the reduction-displacement process.

Conclusions

The results presented here provide evidence that using conductive additives in conjunction with an *in situ* reduction-displacement deposition mechanism provides a path toward the ultimate goal of complete electrical contact and full utilization of all electroactive particles in an inherently insulating polyanion framework electroactive cathode material. The use of a combination of *in situ* and *ex situ* spectroscopic and diffraction-based experimental techniques demonstrates an effective approach to determine the conditions under which an optimal electrically conductive network can be formed. Using an *in situ* EDXRD technique we have shown that the use of a conductive additive such as graphite produces a spatially uniform deposition of silver metal in the $Ag_2VP_2O_8$ cathode upon electrochemical reduction-displacement in lithium based batteries. Unlike the $Ag_2VP_2O_8$ cathodes without graphite, the amount of silver metal formed by reduction-displacement deposition in the composite C-$Ag_2VP_2O_8$ cathodes is independent of discharge rate, as determined by *ex situ* x-ray diffraction and x-ray absorption measurements.

Interestingly, there are significant differences in the AC impedance response for Li/C-$Ag_2VP_2O_8$ cells discharged at different rates. Via diffraction measurements a notable difference between the silver metal deposition in fast- and slow-discharged cells is the size of the silver metal nanoparticles; at the higher discharge rate the silver metal nanoparticles are smaller than those produced while discharging more slowly. Even though the volume of silver

deposited is the same, the smaller silver metal particles are more effective at producing a conductive network than the larger silver metal particles, resulting in a lower impedance and more complete utilization of the electroactive material, as depicted schematically in Fig. 8. Thus, these results suggest a new, non-intuitive paradigm for decreasing the overall impedance of battery electrodes which are designed for *in situ* conductivity enhancement via reduction-displacement deposition; initially discharge the cathode a very small amount at a very high rate, thereby depositing smaller silver metal particles and forming a more effective silver metal network at each particle of electroactive material, in order to enhance the conductivity and improve the subsequent electrochemical function of the cell. The cell could be then discharged as required by the specific application with the benefits of enhanced current capability and realized capacity from appropriate priming prior to application-specific use. These results highlight the benefit of using cathode materials employing a reduction-deposition of silver metal in tandem with conductive additives. By combining cathode materials that create their own conductive network with conductive additives, optimal and controllable electrochemical function can be achieved.

In our study we show that the addition of carbon does improve performance as expected, however we demonstrate that the addition of carbon is not the only effect that can enhance the performance of these batteries. By using a faster discharge rate early in the lifetime of the cell, we show that a more effective conductive network can be created not by simply increasing the amount of conductive material, silver metal, that is present, but by changing the particle size and the effective conductor/active material interface. We demonstrate that by increasing the interfacial area between the conductor and the active material we can reduce the electrochemical impedance more effectively and allow for greater rate capability. This will affect the polarization and therefore the energy density necessary for high power applications.

While the effect of carbon additives in a composite electrode is to provide conductive pathways for electron access, this study directly demonstrates that simply reaching a percolation threshold in an electrode is not sufficient. In addition to decreasing the overall resistance of the electrode, the conductive networks in an electrode containing a nonconducting active material must provide conducting pathways to each electroactive particle to allow for full utilization of the active material. The challenge with regard to electrode design is how to do this volumetrically efficiently.

While the studies were conducted on a specific class of materials, $Ag_wV_xO_yPO_z$, the study has broader implications in terms of composite electrode design. The $Ag_wV_xO_yPO_z$ materials are appropriate model systems for these studies as the conductive pathways are formed by silver, Ag, a high Z material where their formation can be followed by diffraction. However, the conclusions apply to the design of all composite electrodes. Most electroactive materials (i.e. oxides and phosphates) are inherently insulating, and could benefit from a related approach incorporating small quantities of conductive materials applied appropriately to improve interparticle contact.

Acknowledgements

This work was supported as part of the Center for Mesoscale Transport Properties, an Energy Frontier Research Center supported by the U.S. Department of Energy, Office of Science, Basic Energy Sciences, under award #DE-SC0012673. Use of the National Synchrotron Light Source beamlines X17B1 and X11A was supported by DOE contract DE-AC02-98CH10886. K. C. Kirshenbaum acknowledges postdoctoral support from Brookhaven National Laboratory and the Gertrude and Maurice Goldhaber Distinguished Fellowship Program. We thank M. C. Croft for helpful discussions and K. Pandya for assistance with XAS measurements.

Notes and references

[a] Energy Sciences Directorate, Brookhaven National Laboratory, Upton, NY 11973, USA
[b] Department of Chemistry, Stony Brook University, Stony Brook, NY 11794, USA
[c] Department of Materials Science and Engineering, Stony Brook University, Stony Brook, NY 11794, USA
*Corresponding authors: (A.C.M.) amy.marschilok@stonybrook.edu; (K.J.T.) kenneth.takeuchi.1@stonybrook.edu, (E.S.T.) esther.takeuchi@stonybrook.edu

1. N. J. Dudney and J. Li, *Science*, 2015, 347, 131-132.
2. R. Cornut, D. Lepage and S. B. Schougaard, *Journal of the Electrochemical Society*, 2012, 159, A822-A827.
3. J. L. Li, B. L. Armstrong, C. Daniel, J. Kiggans and D. L. Wood, *J. Colloid Interface Sci.*, 2013, 405, 118-124.
4. J. J. Yun, Y. Wang, T. Gao, H. Y. Zheng, M. Shen, Q. T. Qu and H. H. Zheng, *Electrochim Acta*, 2015, 155, 396-401.
5. E. S. Takeuchi, A. C. Marschilok, K. Tanzil, E. S. Kozarsky, S. Zhu and K. J. Takeuchi, *Chemistry of Materials*, 2009, 21, 4934-4939.
6. E. S. Takeuchi, C.-Y. Lee, P.-J. Cheng, M. C. Menard, A. C. Marschilok and K. J. Takeuchi, *Journal of Solid State Chemistry*, 2013, 200, 232-240.
7. K. C. Kirshenbaum, D. C. Bock, Z. Zhong, A. C. Marschilok, K. J. Takeuchi and E. S. Takeuchi, *Physical chemistry chemical physics : PCCP*, 2014, 16, 9138-9147.
8. S. I. Lee, Y. Song, T. W. Noh, X. D. Chen and J. R. Gaines, *Phys Rev B*, 1986, 34, 6719-6724.
9. G. Liang, M. C. Croft and Z. Zhong, *Journal of the Electrochemical Society*, 2013, 160, A1299-A1303.
10. E. S. Takeuchi, A. C. Marschilok, K. J. Takeuchi, A. Ignatov, Z. Zhong and M. Croft, *Energ Environ Sci*, 2013, 6, 1465-1470.
11. W. A. Paxton, Z. Zhong and T. Tsakalakos, *J Power Sources*, 2015, 275, 429-434.
12. J. Russenbeek, Y. Gao, Z. Zhong, M. Croft, N. Jisrawi, A. Ignatov and T. Tsakalakos, *J Power Sources*, 2011, 196, 2332-2339.
13. N. V. Y. Scarlett, I. C. Madsen, J. S. O. Evans, A. A. Coelho, K. McGregor, M. Rowles, M. R. Lanyon and A. J. Urban, *J Appl Crystallogr*, 2009, 42, 502-512.
14. K. Kirshenbaum, D. C. Bock, C.-Y. Lee, Z. Zhong, K. J. Takeuchi, A. C. Marschilok and E. S. Takeuchi, *Science*, 2015, 347, 149-154.
15. Z. L. Liu, J. Y. Lee and H. J. Lindner, *J Power Sources*, 2001, 97-8, 361-365.
16. J. K. Hong, J. H. Lee and S. M. Oh, *J Power Sources*, 2002, 111, 90-96.
17. A. Daidouh, M. L. Veiga and C. Pico, *Journal of Solid State Chemistry*, 1997, 130, 28-34.

18. M. E. Spahr, D. Goers, A. Leone, S. Stallone and E. Grivei, *J Power Sources*, 2011, 196, 3404-3413.
19. J. Li and J. K. Kim, *Compos Sci Technol*, 2007, 67, 2114-2120.
20. B. Ravel and M. Newville, *Journal of Synchrotron Radiation*, 2005, 12, 537-541.
21. C. A. Schneider, W. S. Rasband and K. W. Eliceiri, *Nat. Methods*, 2012, 9, 671-675.
22. H. C. Shin, W. I. Cho and H. Jang, *Electrochim Acta*, 2006, 52, 1472-1476.
23. J. W. Gallaway, M. Menard, B. Hertzberg, Z. Zhong, M. Croft, L. A. Sviridov, D. E. Turney, S. Banerjee, D. A. Steingart and C. K. Erdonmez, *Journal of the Electrochemical Society*, 2015, 162, A162-A168.
24. F. C. Strobridge, B. Orvananos, M. Croft, H.-C. Yu, R. Robert, H. Liu, Z. Zhong, T. Connolley, M. Drakopoulos, K. Thornton and C. P. Grey, *Chemistry of Materials*, 2015, 27, 2374-2386.
25. R. D. Doherty, *Prog Mater Sci*, 1997, 42, 39-58.
26. R. D. Doherty, D. A. Hughes, F. J. Humphreys, J. J. Jonas, D. J. Jensen, M. E. Kassner, W. E. King, T. R. McNelley, H. J. McQueen and A. D. Rollett, *Mat Sci Eng a-Struct*, 1997, 238, 219-274.
27. D. C. Bock, A. C. Marschilok, K. J. Takeuchi and E. S. Takeuchi, *J Power Sources*, 2013, 231, 219-225.
28. D. C. Bock, K. J. Takeuchi, A. C. Marschilok and E. S. Takeuchi, *Dalton T*, 2013, 42, 13981-13989.
29. S. Calvin and K. E. Furst, *XAFS for everyone*, CRC Press, Boca Raton, 2013.
30. C. J. Patridge, C. Jaye, T. A. Abtew, B. Ravel, D. A. Fischer, A. C. Marschilok, P. Zhang, K. J. Takeuchi, E. S. Takeuchi and S. Banerjee, *Journal of Physical Chemistry C*, 2011, 115, 14437-14447.

